THE JOURNAL OF PHYSICAL CHEMISTRY C

Article

pubs.acs.org/JPCC

Side-by-Side Assembly of Gold Nanorods Reduces Ensemble-Averaged SERS Intensity

Anna Lee,[†] Aftab Ahmed,[‡] Diego P. dos Santos,[‡] Neil Coombs,[†] Jai Il Park,[†] Reuven Gordon,*[,‡] Alexandre G. Brolo,*[,§] and Eugenia Kumacheva*[,†]

[†]Department of Chemistry, University of Toronto, 80 Saint George Street, Toronto, Ontario M5S 3H6, Canada

[§]Department of Chemistry, University of Victoria, P.O. Box 3065, Victoria, British Columbia, V8W 3 V6, Canada

[‡]Department of Electrical and Computer Engineering, University of Victoria, Victoria, British Columbia, V8W 3P6, Canada

Supporting Information

ABSTRACT: It is generally expected that aggregates of metal nanoparticles are more efficient surface-enhanced Raman scattering (SERS) probes than individual nanoparticles, due to the enhancement of the electric field in the interparticle gaps. We show that, for asymmetric nanoparticles, such as gold nanorods (NRs), this is not always the case: the plasmonic behavior of NRs depends on the mutual orientation of the NRs in the ensemble. We report the results of experimental studies and theoretical analysis of the optical properties of clusters of side-by-side assembled gold NRs. Ensemble-averaged SERS spectroscopy showed a reduction in SERS intensity. Comprehensive finite-difference time-domain simulations showed a reduction of electric field intensity as the number of NRs per cluster increased. This is due to destructive interference as the radial component of the surface plasmon modes of the NRs in the cluster interact with each other. The present work expands our understanding of the configuration-specific optical behavior of asymmetric gold nanoparticles. Furthermore, it offers guidance toward the "design rules" for the development of colloidal NR systems for sensing applications.

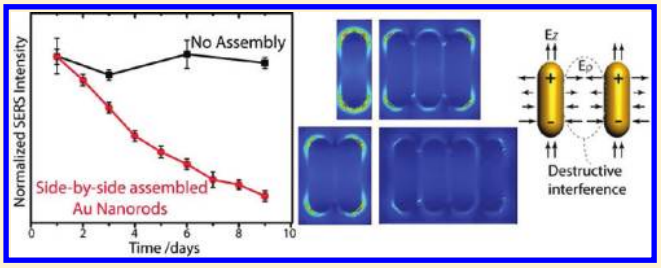

1. INTRODUCTION

The utilization of light−metal interactions at the nanoscale shows promising applications in nanoantennas,[1−5] extraordinary transmission,[6,7] and plasmonic waveguides,[8−10] all of which can be realized through precise control of the architecture, dimensions, and composition of metallic nanostructures. In parallel to "top-down" nanofabrication, "bottom-up" methods utilizing colloidal metallic nanoparticles (MNPs) as the building blocks are receiving increasing attention, because of the low cost of the fabrication and their potential use in vivo.[11−14]

One of the important applications of the plasmonic properties of MNPs is their utilization in surface-enhanced Raman scattering (SERS), which provides structural information about analytes adsorbed on the surface of MNPs and offers exceptionally high sensitivity as compared with ordinary Raman scattering.[15−19] The amplification of Raman intensity arises from local electromagnetic field enhancement due to the surface plasmon resonance (SPR) of MNPs. The magnitude of the Raman scattering from analytes in close proximity to the surface of MNPs is approximately proportional to the fourth power of the local field at the excitation frequency, when the electromagnetic mechanism of SERS is considered.[15,20,21]

The spectral position of the SPR of MNPs can be tuned by varying the dimensions and shapes of MNPs, as well as the nature of the surrounding medium. There is also significant interest in ensembles of MNPs, owing to the coupling of plasmons of adjacent particles.[9,22] Structural, configuration-dependent, plasmonic behavior of ensembles of MNPs can affect both the intensity and the spectral position of the SPR wavelength, thereby providing greater insight into the utilization of the plasmon coupling phenomena.

Currently, the majority of experimental studies of SERS properties of clusters of MNPs have been carried out for irregular, aggregated systems. These structures exhibited a significant variability in their optical properties. As a result, there remains an insufficient understanding of the influence of the architecture of aggregates of MNPs on their SERS properties, particularly, in a solution state.

Gold nanorods (NRs) are of particular interest because of their intrinsic shape-anisotropy. They exhibit transverse and longitudinal SPR, which correspond to the coherent electron oscillations perpendicular and parallel to the long NR axis, respectively.[23] The shape-dependent properties of NRs enable spectral tunability of the longitudinal SPR in the near-IR region. In addition, in their ensembles, gold NRs can exhibit a well-defined mutual alignment in a side-by-side or end-to-end manner.[24−27] The surface plasmon coupling between gold NRs

Received: February 1, 2012
Revised: February 14, 2012
Published: February 15, 2012

in their ensembles depends not only on the interparticle distance but also on the mutual orientation of the NRs with respect to each other. Therefore, gold NRs are well suited for the fundamental studies of the optical properties of aggregated NP systems.[18,19,22,24,25,27]

Thus far, many researchers have focused on the "single-particle" scattering measurements of isolated dimers of NRs in a dry state, in which the NRs were arranged in the end-to-end, side-by-side, L-shaped, or T-shaped manner.[24,25] Experimental results showed that the scattering intensity of dimers depends on the polarization direction of the incident light. The maximum intensity was reached, when the polarization was parallel to the long axis of the NRs. These experimental findings were in agreement with plasmon hybridization calculations and finite-difference time-domain (FDTD) simulations.[24] A study of the effect of angular orientations of NRs in dimers fabricated by electron beam lithography showed the dependence of plasmon coupling on NR orientation, separation, induced dipole strength, and the dielectric constant of the medium.[28] "Single-particle" measurements of scattering, extinction, and SERS of NR dimers and a theoretical explanation of geometry-specific NR assembly[26] have provided a deeper insight into the optical behavior of isolated NP aggregates.[29] Yet, currently, a comprehensive understanding of the optical properties of ensemble-averaged system behavior, factoring in aggregate populations, SPR shift, and electric field (E field) distribution in a dynamic solution-based assembly remains challenging. A small piece of this puzzle has been addressed by our previous work, in which the optical properties of chains of NRs assembled in the end-to-end manner were reported.[30] Specifically, we studied the localized E-field intensity regions ("hot spots") that were generated between the ends of adjacent NRs[31,32] and showed a direct correlation between extinction and ensemble-averaged SERS, as a function of the average aggregation number of NR chains during their assembly.[30] The calculated E-field intensity showed a decrease as the average length of NR chains increased beyond trimers, due to a "trade-off" between losses and local field enhancement. For the end-to-end NR alignment, the E field is oriented along the NR axis, and the near E fields couple constructively, thereby leading to a red shift of the longitudinal SPR.[24,25]

With respect to side-by-side assembly of gold NRs, a number of methods have been demonstrated,[33] including the use of chelating agents,[34] an antibody to a toxin molecule (microcystin-LR),[35] and the addition of anions via electrostatic interactions (citrate).[36] However, to date, only a single experimental study exists that reports on the solution-state SERS properties of side-by-side assembled NRs. This study showed a 10-fold increase in intensity of the SERS signal of the resonant dye, as compared with the SERS of the individual NRs.[36] While we note that 3D multilayered stacks and 2D superstructures are highly SERS-active,[34,37,38] these structures have a distinct E-field distribution and, consequently, different SERS properties, in comparison with small solution-based side-by-side assembled NR clusters. For this reason, the results of our work cannot be directly compared with those of superstructures.

Here, we report experimental and theoretical analyses of the optical properties of side-by-side assembled gold NR clusters. Experimentally, we examined the extinction and ensemble-averaged SERS properties of the NR clusters following their assembly in the solution state. Our results showed a blue shift of SPR wavelength, as expected, but surprisingly, a reduction of SERS intensity. Finite-difference time-domain (FDTD) simulations[39] confirmed the reduction in E-field intensity, as the number of NRs per cluster increases, due to destructive interference between the E-field radial components.

2. MATERIALS AND METHODS

2.1. Synthesis of Gold Nanorods. All chemicals were purchased from Sigma Aldrich (Canada) and used without further purification. Cetyltrimethylammonium bromide (CTAB)-coated gold NRs were synthesized by the "seed-mediated growth method" devised by El-Sayed et al.[40] Briefly, seed solution was prepared by the reduction of $HAuCl_4$, dissolved in an aqueous solution of CTAB, with cold sodium borohydride ($NaBH_4$). The growth solution was prepared by dropwise addition of ascorbic acid into an aqueous solution of $HAuCl_4$, CTAB, and $AgNO_3$. To initiate NR growth, a 5 min-aged seed solution was injected into the growth solution and incubated for 10 h at 27 °C. The resultant CTAB-coated gold NRs were purified by two centrifugation cycles at 8500 rpm for 30 min (*Eppendorf* centrifuge 5417R).

2.2. Side-by-Side Assembly of Gold Nanorods. The site-specific ligand exchange of CTAB was carried out at the NR ends with thiol-terminated polystyrene (SH-PS), purchased from Polymer Science Inc.) with a molecular weight of 12 000 g/mol and a polydispersity index of 1.09.[33] Approximately 0.5 mL of the concentrated aqueous solution of CTAB-coated NRs (~1.0 mg/mL) was rapidly injected under sonication (42 kHz ± 0.6%) into 10 g of tetrahydrofuran (THF) solution containing 5 mg of SH-PS (~0.05 wt %).[30] The solution mixture was sonicated for 30 min and incubated at room temperature for ~24 h. Purification of the sample from free polymer was carried out by eight centrifugation cycles at 8500 rpm for 30 min, and THF was used as a solvent. This purified sample was used as a stock NR solution. Next, 3 μM of a Raman reporter, cresyl violet (CV), was introduced into 990 μL of the stock solution under shaking. Following a 30 min agitation under gentle vortex conditions, the mixture was incubated for 1 h. To trigger side-by-side NR assembly, we added dropwise a THF−water mixture containing 10 vol % of water. All subsequent physical measurements were carried out on the same batch of NRs. As soon as NR self-assembly began, we carried out all subsequent physical measurements in parallel.

2.3. Characterization. The evolution of the side-by-side NR assemblies was monitored by using a Cary 500 UV/vis/near-IR spectrophotometer. Extinction spectra were recorded in the spectral range from 400 to 1200 nm at room temperature by using a 1 cm path length cell. Scanning transmission electron microscopy (STEM) images were recorded with a Hitachi S-5200 field emission SEM equipped with a transmitted electron detector. The surface-enhanced Raman scattering (SERS) measurements were carried out by using a compact Raman system (Advantage Raman Series, DeltaNu) (785 nm laser line, the laser beam diameter of 35 μm at the focal point). The intensity of SERS was calibrated and normalized to the Raman spectra of cyclohexane and polystyrene, in order to correct for variations in optical alignment and instrument response. The spectra were acquired with a 5 cm^{-1} resolution. Control SERS measurements of CV adsorbed from either THF or water on a roughened gold substrate were conducted by using a Renishaw InVia System spectrometer coupled to a Leica microscope. The laser excitation and power were 785 nm (Renishaw solid-state laser model HPNIR785) and ~8 mW, respectively. The spectra were measured using a 20× objective (NA = 0.4) with an

dx.doi.org/10.1021/jp3010597 | J. Phys. Chem. C 2012, 116, 5538−5545

exposure time of 10 s and 5 scans. A solid gold electrode was roughened with 25 successive oxidation and reduction cycles from 0.3 to 1.2 V in an aqueous 0.1 M KCl working solution. A platinum wire was used as a counter electrode, and the reference electrode was Ag|AgCl|KCl(sat). The roughened gold electrode was then isolated from the electrochemical cell, and CV in THF or water was introduced for the SERS measurements.

2.4. Finite-Difference Time-Domain (FDTD) Simulations. To model the complex permittivity of gold, we used the experimental data of Johnson and Christy.[41] The simulation domain was terminated by a perfectly matched layer to ensure minimum reflections from the boundaries of the simulation domain. The total field scattered field (TFSF) source was used for the determination of absorption, scattering, and extinction cross sections of assembled NRs, which divided the simulation domain into two regions. In one region, only scattered fields were present, while the other region contains both the incident and the scattered fields. The scattering cross section was determined by calculating the Poynting vector over a closed surface surrounding the NRs in the scattered field region. The absorption cross section was calculated by determining the net flow of power into a closed surface surrounding the NRs in the total field region. The incident plane wave was polarized at 45° to the long axis of the NRs, and as such, this polarization probes both the transverse and the longitudinal SPR. The mesh override region was defined with a mesh size of 1 nm for accurate modeling of the cylindrical structure in a Cartesian coordinate system.

3. RESULTS AND DISCUSSION

By exploiting the anisotropy of the NRs in shape and surface energy,[42−44] we carried out site-specific exchange of CTAB at the NR ends with thiol-terminated polystyrene SH-PS.[33] The SH-PS tethered to the NR ends rendered the NRs analogous to an "amphiphilic" molecular species with a hydrophilic long side and hydrophobic end groups. Later in the text, we refer to the PS-functionalized NRs as the "NRs", unless otherwise stated. We triggered the self-assembly of the NRs in a side-by-side manner by changing the quality of solvent for the ligands. We note that THF is a poor solvent for CTAB, and the stability of the NRs in THF was attributed to the polystyrene ligands (the values of the second virial coefficient, A_2, is 9.0×10^{-4} mol cm^3 g^{-2}, equivalent to Flory−Huggins interaction parameter equal to 0.4).[33] We added water to the THF solution of the NRs to a total concentration of water of 10 wt %, thereby reducing the solubility of the PS ligands. As a result, the NRs assembled in the side-by-side manner (Figure 1).

Figure 2a shows photographs of the solutions of NRs following their self-assembly over time. The typical color of the solutions changed from reddish-purple to blue. We did not observe any apparent "precipitation" throughout the acquisition of all measurements. The NR ensembles showed colloidal and temporal stability for at least 3 months. Figure 2b shows the evolution of extinction spectra of NR solutions, plotted over the course of assembly. The consistent blue shift of the longitudinal SPR peak from 770 to 715 nm indicated that the NRs were assembled in a side-by-side configuration.[26] The blue shift occurred due to the parallel alignment of dipole modes of individual NRs (this result will be addressed below by numerical simulations).[24] We did not observe SPR peak broadening, which could be characteristic for the formation of large, irregular NR aggregates. The transverse SPR showed a relatively small red shift from 510 to 519 nm, due to attractive interaction between NRs.

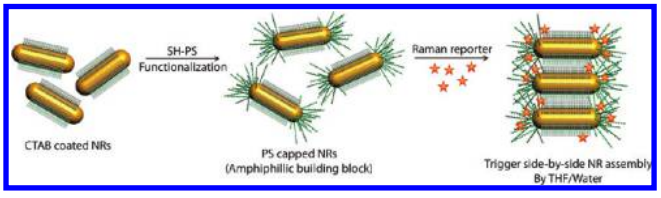

Figure 1. Schematic illustration of the side-by-side NR assembly. A SH-PS is attached to the ends of CTAB-coated gold NRs in THF via site-specific ligand exchange. After the addition of the Raman reporter, the side-by-side assembly was triggered by the addition of water (10 vol %).

Representative scanning transmission electron microscopy (STEM) images of the NR clusters in various stages of their self-assembly are shown in Figure 2a (low-magnification STEM images of the NR assemblies are presented as Figure S1 in the Supporting Information). Using image analysis, we determined that, throughout the self-assembly process, the average distance between the long sides of adjacent NRs remained at 1.97 ± 0.48 nm. This inter-NR spacing was smaller than would be expected for four layers of CTAB ligands (~4 nm, assuming capping of the NR sides with a CTAB bilayer),[45,46] presumably, due to the interdigitation of CTAB molecules in the gaps between the NRs.[47,48]

We did not calculate the average aggregation number of the NR ensembles, because it is well established that, upon evaporation of the solvent on a carbon-coated TEM grid, gold NRs form stacks, in which they are aligned in the parallel manner.[47] The alignment occurs due to the van der Waals forces acting between the NRs: on the basis of Hamaker integral approximation, for small NR separation distance, the side-by-side configuration is preferred.[49] Nevertheless, inspection of the TEM images showed that the number of individual NRs decreased through the course of self-assembly. For example, 24 h after triggering the self-assembly, we observed ~57% of individual NRs, 28% of dimers, 10% of trimers, and 3% of tetramers, whereas for 216 h long assembly, the fractions of these species were 30, 44, 18, and 8%, respectively.

Concurrently, with extinction measurements over the course of side-by-side assembly of the NRs, we monitored ensemble-averaged SERS of cresyl violet (CV) (Figure 3a). The most enhanced SERS bands of CV appeared at 535 and 595 cm^{-1} and were caused by *in plane* vibrational ring modes of CV.[50] The band at 900 cm^{-1} corresponded to the ring "breathing" mode of THF[51] and was used as an internal standard. The position of the bands shown in the SERS spectrum were in accordance with the ordinary Raman spectrum of CV, which suggested that CV was physically adsorbed on the surface of the NRs. Figure 3b shows the variation in the normalized SERS peak intensity of CV at 535 and 595 cm^{-1}, plotted as a function of self-assembly time, t. We observed a gradual reduction in normalized SERS intensities of both peaks of CV for t increasing from 5 min to 216 h. In the control experiment, the spectrum of the solution containing the same amount of CV and individual (not assembled) NRs showed relatively constant intensities of the SERS peak at 595 cm^{-1} for the duration up to 216 h.

To further investigate the experimental findings, we conducted comprehensive electromagnetic FDTD simulations, numerically solving Maxwell's equations by iteration over time.

dx.doi.org/10.1021/jp3010597 | J. Phys. Chem. C 2012, 116, 5538−5545

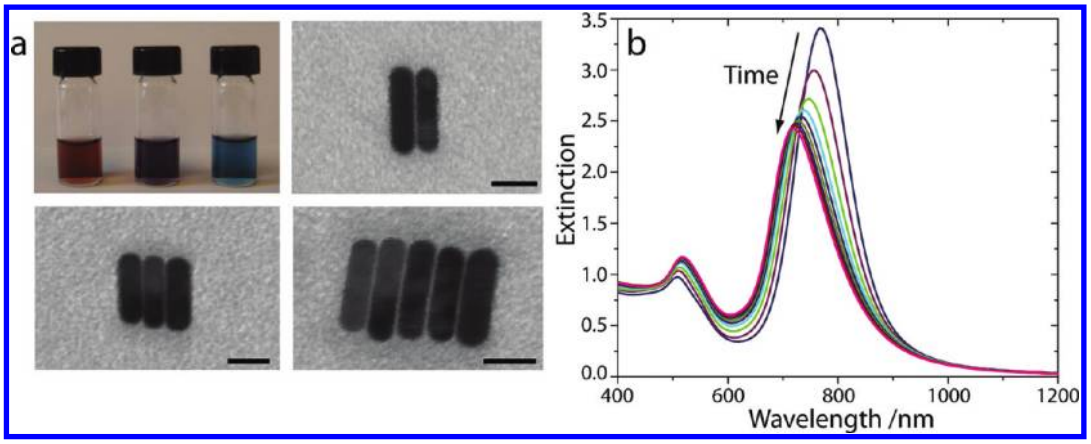

Figure 2. (a) A photograph showing a typical change in color of the solution of self-assembling NRs as a function of time from reddish-purple to blue (top left). Representative scanning transmission electron microscopy (STEM) images of NRs in various stages of self-assembly. The scale bar is 15 nm. (b) Variation in extinction properties of NR ensembles over time.

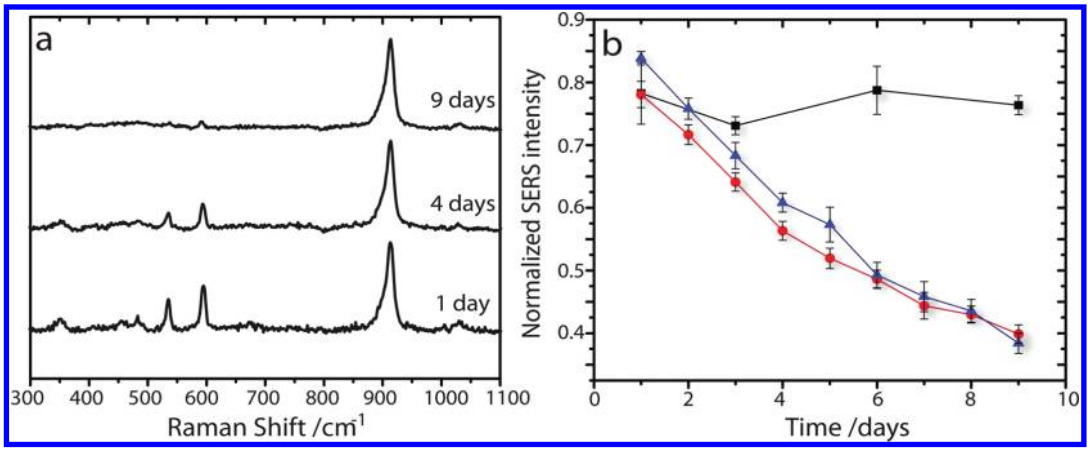

Figure 3. (a) Representative ensemble-averaged SERS spectra of cresyl violet (CV), measured in the course of side-by-side assembly of the NRs as a function of time. The band at 900 cm^{-1} corresponds to THF and was used as an internal standard to normalize the intensity of SERS of CV at 535 and 595 cm^{-1}. (b) Normalized SERS intensity at 535 cm^{-1} (red circle), 595 cm^{-1} (blue triangle), and in control experiments conducted without the assembly of the NRs (black square, for SERS of CV at 595 cm^{-1}) as a function of time.

Figure 4a–c shows FDTD calculations of the change in the normalized absorption, scattering, and extinction cross sections, all plotted as a function of wavelength for the assemblies with a side-by-side NR alignment. The number of NRs in the clusters changed from one to eight NRs.

By comparing the results obtained in experiments and simulations, we observed a small difference in the spectral position and the relative intensity of the transverse SPR of the NRs. The SPR modes are dependent on the direction of propagation of incident radiation. The simulations were carried out for one direction of propagation incident wavevector (k_{inc}), which was perpendicular to the long axis of the NRs. This was not the case for the extinction experiments carried out for the NR solution. To verify the dependence on the propagation direction, we carried out simulations for two different directions of light propagation, that is, parallel and perpendicular to the long axis of the NRs (Supporting Information, Figure S2). We note that, for the parallel propagation, only the transverse SPR is excited.

The FDTD simulation showed a blue shift of the resonance wavelength from 779 to 653 nm, as the number of NRs per ensemble increased from one to eight NRs, respectively. The resonance wavelength of a single NR or a stack of NRs arranged in a side-by-side manner is determined by two variables: the propagation constant β of the radial SP mode and the phase of light reflection from the ends of the NRs. At resonance, the following condition is satisfied[2,29,52]

$$\beta L + \phi_{ref} = \pi \quad (1)$$

where L is the NR length, ϕ_{ref} is the phase of reflection from the end of the NRs, and β is the propagation constant ($\beta = n_{eff} 2\pi/\lambda$, where n_{eff} is the effective index of the system containing NRs and the surrounding medium). The analytical expression for the phase of reflection from flat-ended NRs has recently been derived,[53] whereas only numerical solutions for phase of reflection for NRs with hemispherical ends (common in colloidal systems) are currently available.

The value of β is a geometry-dependent variable, and it can be obtained from the mode shape of the radial SP wave. Figure 5 shows mode shapes of one NR and side-by-side assemblies of two and three NRs. By using modal solutions, we numerically verified that, as the number of NRs in the ensemble increases, the value of n_{eff} decreases, thereby reducing the value of β. More specifically, for one, two, and three NRs, the resultant value of n_{eff} was 11.81, 9.29, and 8.13, respectively, and the corresponding value of β was 98.9 × 10^6, 77.8 × 10^6, and 68.1 × 10^6 m^{-1}, respectively.

dx.doi.org/10.1021/jp3010597 | J. Phys. Chem. C 2012, 116, 5538–5545

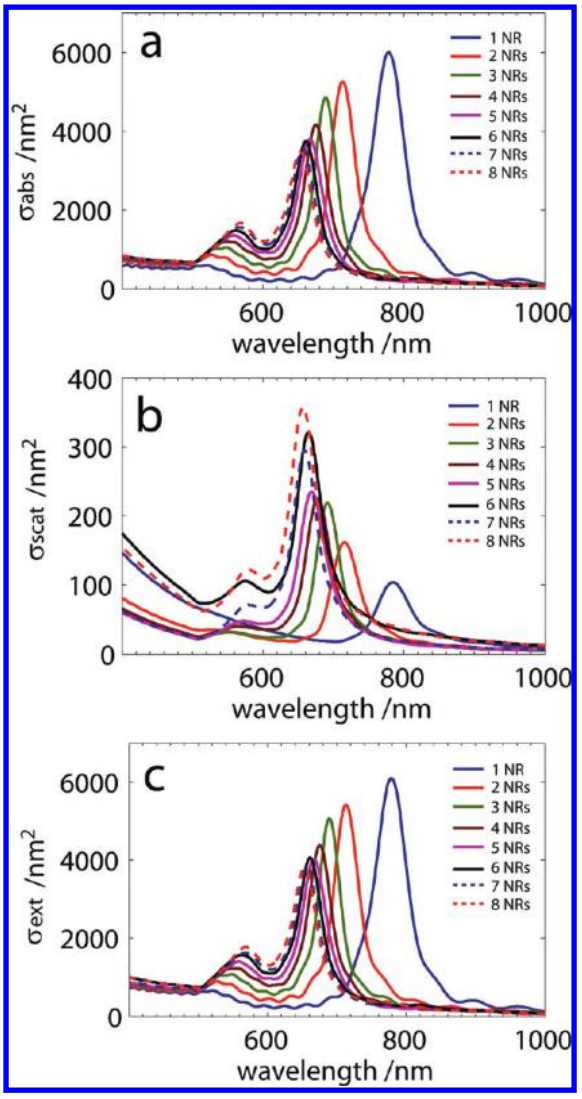

Figure 4. Calculated normalized absorption (a), scattering (b), and extinction cross section (c), all plotted as a function of wavelength for NR assemblies containing from one to eight NRs. Simulations were carried out using FDTD.

This reduction occurs when the NRs are brought into close proximity to each other in the side-by-side ensembles. Consequently, the mode shape of interacting NRs changed as compared with that of an individual NR. The radial components of the E field of the neighboring NRs cancel each other, due to destructive interference, resulting in a reduction of the local E field (Figure 6). To satisfy eq 1, the reduction in n_{eff} had to be compensated by a proportional amount of reduction in the resonant wavelength (to first order, ignoring the effects of dispersion in n_{eff}). Therefore, a blue shift occurred as the number of NRs aligned in a side-by-side manner increased (it should be noted that ϕ_{ref} is weakly wavelength-dependent,[53] and earlier work[2] suggested that $\phi_{ref} \approx 0$).

Figure 7a–e shows examples of FDTD simulations of E-field intensity profiles of ensembles containing from one to five NRs at their corresponding resonance wavelengths at 780, 713, 690, and 678 nm, respectively (additional simulations are provided in the Supporting Information, Figure S3). We note that the field intensity in the gap between two neighboring NRs is significantly smaller, compared with the field intensity for a single NR. Figure 7e shows the normalized sum of E-field intensity squared as a function of wavelength. As the number of NRs per stack increased from one to eight, the sum of the intensity squared decreased. Unlike end-to-end NR assembly, which exhibited constructive inference,[30] for the side-by-side assembly, the reduction of the field originated from the cancellation of the radial component of the SP mode, thereby leading to destructive interference, as shown in Figure 6. We note that we examined the E-field intensity of two different geometries of NR assemblies, that is, the 2D "stack" vs a 3D "bundle",[54] and found similar sums of E-field intensities (Supporting Information, Figure S4).

The results presented in Figures 5–7 suggest that, due to destructive interference, the region between the rods is not the "hot spot". To validate this experimentally, we conducted control SERS measurements of CV adsorbed from either THF or water on a roughened gold substrate.[55] Figure 8 shows that the SERS spectra of CV are solvent-dependent.

In the THF solution, the spectral positions of the CV peaks (591 cm^{-1}) were in concordance with those observed for CV coassembled with NRs (Figure 3a), whereas in the water environment, CV exhibited a significant shift in the spectral peak positions[52] to 541 and 600 cm^{-1}, in comparison with those measured in the THF solution. The observed changes may be caused by hydrogen bonding between CV and water molecules, which causes the change in the average orientation of the CV molecules with respect to the surface of NRs. On the basis of the similarity of SERS spectra of CV acquired for its THF solution and for the self-assembled NR clusters, we conclude that, in the side-by-side assembled NR experiments,

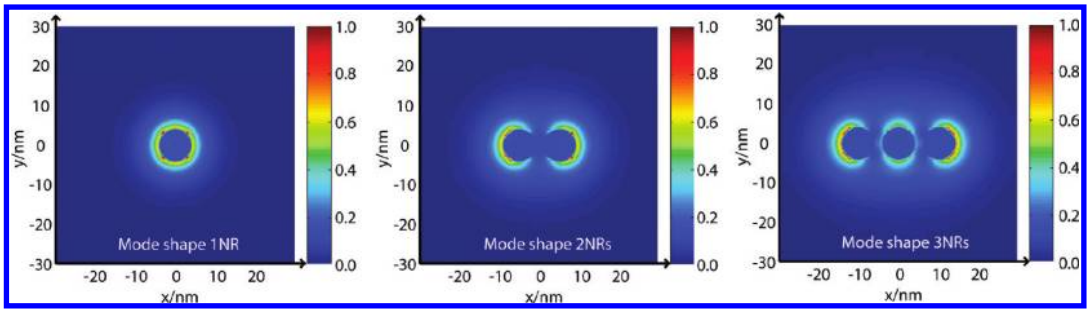

Figure 5. Modes supported by side-by-side assembly of NRs. Mode shapes of surface plasmons of one to three NRs from left to right (looking down the long axis (z axis) of the NRs). The resulting effective index values are used for the calculation of the propagation constant of surface wave in the different geometries and show that the propagation constant decreases as the number of NRs increase. Fields are normalized to their maximum intensities.

dx.doi.org/10.1021/jp3010597 | J. Phys. Chem. C 2012, 116, 5538–5545

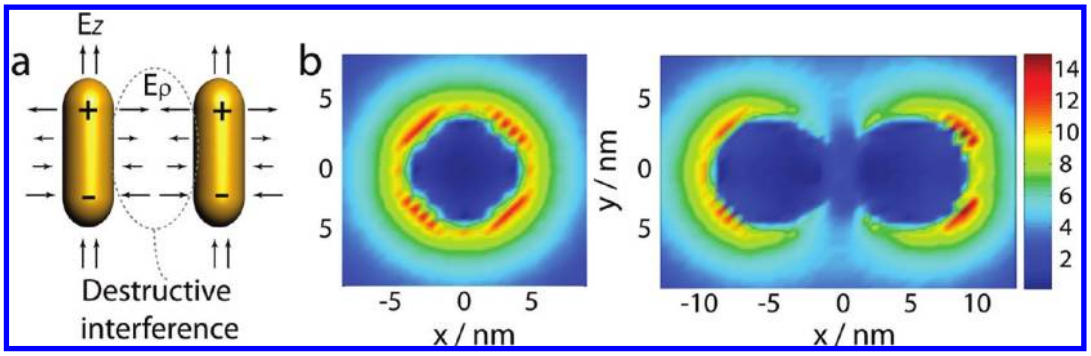

Figure 6. (a) Schematic illustration of gold NRs assembled in a side-by-side manner showing a reduction of electric field due to destructive interference of the radial component of the E field (E_ρ). (b) Radial E-field profile via FDTD simulations for one and two NRs looking down the long axis (z axis) of the NRs showing the field cancellation in the gap between two NRs.

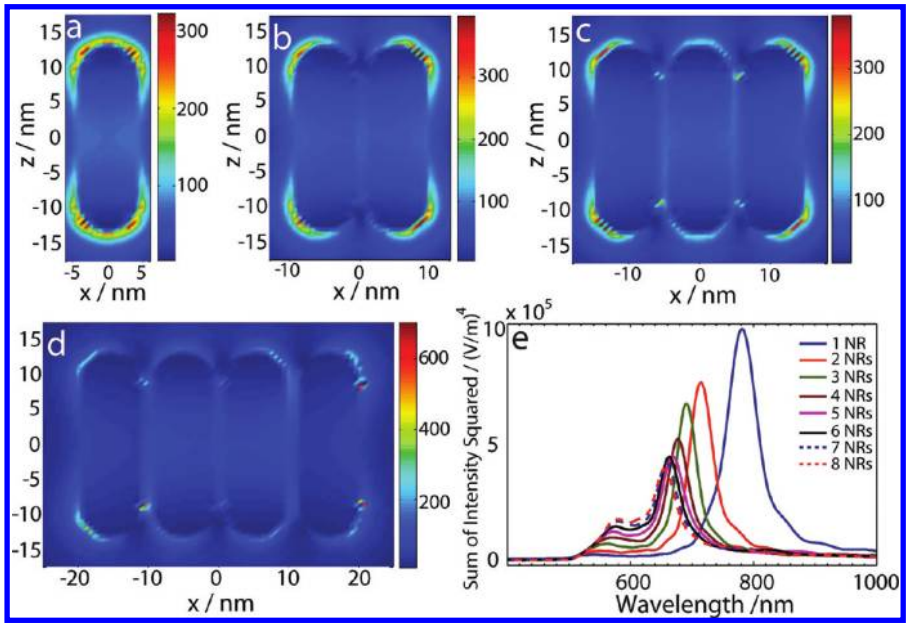

Figure 7. (a–d) Examples of electric field intensity profiles produced via 3D-FDTD simulation for side-by-side assembled NRs at their resonance wavelengths. Polarization of the incident light is at 45° to the long axis (z coordinate) of NRs. (e) Sum of electric field intensity squared of ensembles containing a different number of NRs.

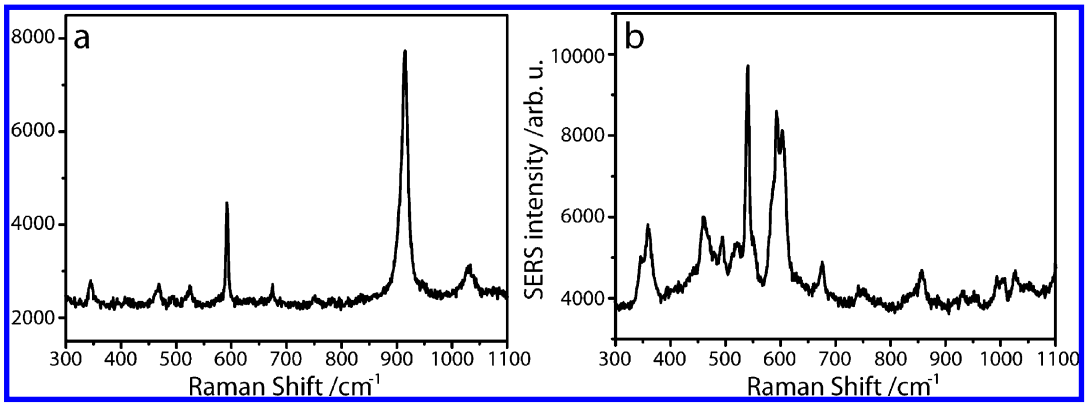

Figure 8. SERS of CV on a roughened gold substrate in THF (a) and water (b). In THF, the spectral positions of the CV peaks (591 cm^{-1}) were in concordance with those observed for CV coassembled with NRs. A 785 nm laser excitation was used.

we are probing SERS properties of CV in a THF environment, from which water is largely excluded. Since the SERS signal originates from the "hot-spot" region, this result suggests that the CV species producing most of the Raman scattered signal are located at the ends of NRs (and not between the NR long sides, where destructive interference is dominant), in agreement with numerical calculations presented in Figure 7. We note that probing of SERS of CV located at the ends of NRs did not exclude the possibility of CV being located on the sides of NRs. Such partition is possible because CV has an

dx.doi.org/10.1021/jp3010597 | J. Phys. Chem. C 2012, 116, 5538–5545

amphiphilic nature, due to the presence of an unsaturated ring structure and a cationic imine group. Thus, the hydrophobic moiety of CV can intercalate into the hydrocarbon chains of the CTAB bilayer on the NR long sides. A similar effect was observed for molecules containing both ionic and hydrophobic moieties (e.g., tetraphenylphosphonium) partitioning into a lipid bilayer, when hydrophobic forces dominated over electrostatic repulsion.[29]

To further support our finding of the reduction of SERS intensity arising from probing at the ends of NRs, we numerically examined location-specific E-field variation at the ends of NRs (Supporting Information, Figure S5). The normalized sum of E-field intensity squared over volume showed a decrease as a function of the number of NRs. The reduction of E field suggested that SERS of CV should decrease as the number of NRs per ensemble increases, considering only the electromagnetic effect of SERS, which was the predominant factor in our work.

In summary, the present study provides an important insight into the optical properties of side-by-side assembled gold NRs. We showed that the normalized sum of the E-field intensity *decreases* as the number of NRs in the ensemble increases. The observed reduction of E-field intensity occurs due to the cancelation of the radial component of SP modes. Calculated and measured extinction spectra show a blue shift of the longitudinal SPR, which is caused by the reduction of effective index, when the number of NRs per ensemble increases. While it is generally expected that aggregates of metal nanoparticles are better SERS platforms than individual nanoparticles, our experimental work showed the reduction in ensemble-averaged SERS intensity, which was in concordance with comprehensive FDTD calculations.

Although there has been significant progress in the organization of NRs in the side-by-side mode, the next challenge is to exploit the functionality of these plasmonic ensembles. While the observed spectral shift in SPR of NRs has found applications in colorimetric sensors, our results suggest that small side-by-side assembled clusters may not be suitable for use as highly sensitive SERS probes. Fundamentally, this study expands our understanding of the interplay between geometry, assembly, and the optical properties of plasmonic nanoparticles.

■ ASSOCIATED CONTENT

Supporting Information

STEM images of side-by-side assembled gold nanorods (NRs); finite-difference time-domain (FDTD) simulations showing absorption, scattering, and extinction of two NRs per stack for two different directions of propagation of incident radiation; examples of electric field profiles of side-by-side assembled gold NR structures via FDTD simulations for five to eight NRs per stack; electric field profiles of the bundle structures containing three and four NRs; and the total volume of the sum of electric field intensity squared for the ends of NR ensembles. This material is available free of charge via the Internet at http://pubs.acs.org.

■ AUTHOR INFORMATION

Corresponding Author

*E-mail: rgordon@uvic.ca (R.G.), agbrolo@uvic.ca (A.G.B.), ekumache@chem.utoronto.ca (E.K.).

Notes

The authors declare no competing financial interest.

■ ACKNOWLEDGMENTS

A.L., A.A., R.G., A.G.B., and E.K. acknowledge financial support of NSERC Canada for the Strategic Network for Bioplasmonic Systems (Biopsys). A.L. thanks Xiaoqiang Zhang for his help. D.P.d.S. acknowledges Inter-American Collaboration in Materials Research (CIAM) grants from NSERC (Canada) and FAPESP (Brazil).

■ REFERENCES

(1) Ahmed, A.; Gordon, R. *Nano Lett.* **2011**, *11*, 1800−1803.
(2) Novotny, L. *Phys. Rev. Lett.* **2007**, *98*, 4.
(3) Curto, A. G.; Volpe, G.; Taminiau, T. H.; Kreuzer, M. P.; Quidant, R.; van Hulst, N. F. *Science* **2010**, *329*, 930−933.
(4) Seok, T. J.; Jamshidi, A.; Kim, M.; Dhuey, S.; Lakhani, A.; Choo, H.; Schuck, P. J.; Cabrini, S.; Schwartzberg, A. M.; Bokor, J.; Yablonovitch, E.; Wu, M. C. *Nano Lett.* **2011**, *11*, 2606−2610.
(5) Taminiau, T. H.; Stefani, F. D.; Segerink, F. B.; Van Hulst, N. F. *Nat. Photonics* **2008**, *2*, 234−237.
(6) Ebbesen, T. W.; Lezec, H. J.; Ghaemi, H. F.; Thio, T.; Wolff, P. A. *Nature* **1998**, *391*, 667−669.
(7) Martin-Moreno, L.; Garcia-Vidal, F. J.; Lezec, H. J.; Pellerin, K. M.; Thio, T.; Pendry, J. B.; Ebbesen, T. W. *Phys. Rev. Lett.* **2001**, *86*, 1114−1117.
(8) Lal, S.; Link, S.; Halas, N. J. *Nat. Photonics* **2007**, *1*, 641−648.
(9) Maier, S. A.; Brongersma, M. L.; Kik, P. G.; Atwater, H. A. *Phys. Rev. B* **2002**, *65*.
(10) Barthes, J.; Francs, G. C. d.; Bouhelier, A.; Weeber, J. C.; Dereux, A. *Phys. Rev. B* **2011**, *84*.
(11) Huang, X.; El-Sayed, I. H.; Qian, W.; El-Sayed, M. A. *Nano Lett.* **2007**, *7*, 1591−1597.
(12) Lee, K. S.; El-Sayed, M. A. *J. Phys. Chem. B* **2006**, *110*, 19220−19225.
(13) Linic, S.; Christopher, P.; Ingram, D. B. *Nat. Mater.* **2011**, *10*, 911−921.
(14) Jain, P. K.; Huang, X.; El-Sayed, I. H.; El-Sayed, M. A. *Acc. Chem. Res.* **2008**, *41*, 1578−1586.
(15) Moskovits, M. *Rev. Mod. Phys.* **1985**, *57*, 783−826.
(16) Aroca, R. *Surface-Enhanced Vibrational Spectroscopy*; John Wiley & Sons: New York, 2006.
(17) Moskovits, M.; Suh, J. S. *J. Phys. Chem.* **1984**, *88*, 5526−5530.
(18) Le Ru, E. C.; Grand, J.; Sow, I.; Somerville, W. R. C.; Etchegoin, P. G.; Treguer-Delapierre, M.; Charron, G.; Félidj, N.; Lévi, G.; Aubard, J. *Nano Lett.* **2011**, *11*, 5013−5019.
(19) Shanmukh, S.; Jones, L.; Driskell, J.; Zhao, Y.; Dluhy, R.; Tripp, R. A. *Nano Lett.* **2006**, *6*, 2630−2636.
(20) Kneipp, K.; Kneipp, H.; Itzkan, I.; Dasari, R. R.; Feld, M. S. *Chem. Rev.* **1999**, *99*, 2957−2975.
(21) Weitz, D. A.; Garoff, S.; Gersten, J. I.; Nitzan, A. *J. Chem. Phys.* **1983**, *78*, 5324−5338.
(22) Halas, N. J.; Lal, S.; Chang, W.-S.; Link, S.; Nordlander, P. *Chem. Rev.* **2011**, *111*, 3913−3961.
(23) Huang, X.; Neretina, S.; El-Sayed, M. A. *Adv. Mater.* **2009**, *21*, 4880−4910.
(24) Slaughter, L. S.; Wu, Y. P.; Willingham, B. A.; Nordlander, P.; Link, S. *ACS Nano* **2010**, *4*, 4657−4666.
(25) Funston, A. M.; Novo, C.; Davis, T. J.; Mulvaney, P. *Nano Lett.* **2009**, *9*, 1651−1658.
(26) Jain, P. K.; Eustis, S.; El-Sayed, M. A. *J. Phys. Chem. B* **2006**, *110*, 18243−18253.
(27) Shao, L.; Woo, K. C.; Chen, H. J.; Jin, Z.; Wang, J. F.; Lin, H. Q. *ACS Nano* **2010**, *4*, 3053−3062.
(28) Tabor, C.; Van Haute, D.; El-Sayed, M. A. *ACS Nano* **2009**, *3*, 3670−3678.
(29) Flewelling, R. F.; Hubbell, W. L. *Biophys. J.* **1986**, *49*, 531−540.

(30) Lee, A.; Andrade, G. F. S.; Ahmed, A.; Souza, M. L.; Coombs, N.; Tumarkin, E.; Liu, K.; Gordon, R.; Brolo, A. G.; Kumacheva, E. *J. Am. Chem. Soc.* **2011**, *133*, 7563−7570.
(31) Lee, S. J.; Morrill, A. R.; Moskovits, M. *J. Am. Chem. Soc.* **2006**, *128*, 2200−2201.
(32) Kumar, J.; Thomas, K. G. *J. Phys. Chem. Lett.* **2011**, *2*, 610−615.
(33) (a) Nie, Z. H.; Fava, D.; Kumacheva, E.; Zou, S.; Walker, G. C.; Rubinstein, M. *Nat. Mater.* **2007**, *6*, 609−614. (b) Nie, Z. H.; Fava, D.; Winnik, M. A.; Rubinstein, M.; Kumacheva, E. *J. Am. Chem. Soc.* **2008**, *130*, 3683. (c) Fava, D.; Nie, Z. H.; Winnik, M. A.; Kumacheva, E. *Adv. Mater.* **2008**, *20*, 4318−4322.
(34) Sreeprasad, T. S.; Pradeep, T. *Langmuir* **2011**, *27*, 3381−3390.
(35) Wang, L.; Zhu, Y.; Xu, L.; Chen, W.; Kuang, H.; Liu, L.; Agarwal, A.; Xu, C.; Kotov, N. A. *Angew.Chem., Int. Ed.* **2009**, *49*, 5472−5475.
(36) McLintock, A.; Hunt, N.; Wark, A. W. *Chem. Commun.* **2011**, *47*, 3757−3759.
(37) Yun, S.; Oh, M. K.; Kim, S. K.; Park, S. *J. Phys. Chem. C* **2009**, *113*, 13551−13557.
(38) Alvarez-Puebla, R. A.; Agarwal, A.; Manna, P.; Khanal, B. P.; Aldeanueva-Potel, P.; Carbo-Argibay, E.; Pazos-Perez, N.; Vigderman, L.; Zubarev, E. R.; Kotov, N. A.; Liz-Marzan, L. M. *Proc. Natl. Acad. Sci. U.S.A.* **2011**, *108*, 8157−8161.
(39) Taflove, A; Hagness, S. C. *Computational Electrodynamics: The Finite-Difference Time Domain Method*, 2nd ed.; Artech House: Boston, 2000.
(40) Nikoobakht, B.; El-Sayed, M. A. *Chem. Mater.* **2003**, *15*, 1957−1962.
(41) Johnson, P. B.; Christy, R. W. *Phys. Rev. B* **1972**, *6*, 4370−4379.
(42) Murphy, C. J.; Thompson, L. B.; Chernak, D. J.; Yang, J. A.; Sivapalan, S. T.; Boulos, S. P.; Huang, J.; Alkilany, A. M.; Sisco, P. N. *Curr. Opin. Colloid Interface Sci.* **2011**, *16*, 128−134.
(43) Murphy, C. J.; Thompson, L. B.; Alkilany, A. M.; Sisco, P. N.; Boulos, S. P.; Sivapalan, S. T.; Yang, J. A.; Chernak, D. J.; Huang, J. *J. Phys. Chem. Lett.* **2010**, *1*, 2867−2875.
(44) Liu, K.; Zhao, N.; Kumacheva, E. *Chem. Soc. Rev.* **2011**, *40*, 656−671.
(45) Venkataraman, N. V.; Vasudevan, S. *Proc. Indian Acad. Sci.: Chem. Sci.* **2001**, *113*, 539−558.
(46) Warr, G. G.; Sen, R.; Evans, D. F.; Trend, J. E. *J. Phys. Chem.* **1988**, *92*, 774−783.
(47) Sau, T. K.; Murphy, C. J. *Langmuir* **2005**, *21*, 2923−2929.
(48) Venkataraman, N. V.; Vasudevan, S. *J. Phys. Chem. B* **2001**, *105*, 7639−7650.
(49) Bishop, K. J. M.; Wilmer, C. E.; Soh, S.; Grzybowski, B. A. *Small* **2009**, *5*, 1600−1630.
(50) Vogel, E.; Gbureck, A.; Kiefer, W. *J. Mol. Struct.* **2000**, *550*, 177−190.
(51) Shurvell, H. F.; Southby, M. C. *Vib. Spectrosc.* **1997**, *15*, 137−146.
(52) Xiao, M.; Nyagilo, J.; Arora, V.; Kulkarni, P.; Xu, D.; Sun, X.; Dave, D. P. *Nanotechnology* **2010**, *21*.
(53) Gordon, R. *Opt. Express* **2009**, *17*, 18621−18629.
(54) Side-by-side assembled "bundled" NR structures rather than "stacked" structures can be obtained by the addition of 6 wt % water and 0.2 wt % PS in 10 mL of THF. Nie, Z.; et al. *Nat. Mater.* **2007**, *6*, 609−614 . The "bundled" NR ensembles showed a relatively lower sum of E-field intensity squared as compared with the "stacked" configuration.
(55) Brolo, A. G.; Jiang, Z.; Irish, D. E. *J. Electroanal. Chem.* **2003**, *547*, 163−172.